

---

# FOURIER RNNs FOR SEQUENCE ANALYSIS AND PREDICTION

---

PREPRINT

**Moritz Wolter**  
Institute for Computer Science  
University of Bonn  
wolter@cs.uni-bonn.de

**Angela Yao**  
School of Computing  
National University of Singapore  
ayao@comp.nus.edu.sg

August 30, 2022

## ABSTRACT

Fourier methods have a long and proven track record in as an excellent tool in data processing. We propose to integrate Fourier methods into complex recurrent neural network architectures and show accuracy improvements on analysis and prediction tasks as well as computational load reductions. We predict synthetic data drawn from the synthetic-Lorenz equations as well as real world human motion prediction. We demonstrate the setup’s analysis capabilities on the task of music recognition.

## 1 Introduction

Prior to the popular growth of deep learning approaches, analyzing time series and sequence data in the spectral domain, *i.e.* via a Fourier transform was a standard approach [23, 19, 9]. Fourier analysis disentangles a time domain signal and represents it as a combination of sinusoids. This can greatly simplify the analysis of recurring superimposed patterns in time series data, since in the spectral domain, the single components become elucidated. In addition, the field of harmonic analysis has the backing of hundreds of years of research in applied mathematics, signal processing and electrical engineering.

Currently, these advances are not being fully leveraged by the deep learning community. In particular, as recurrent neural networks (RNNs) become the go-to choice analyzing temporal sequences, it becomes logical to incorporate Fourier transforms directly into the RNN framework. Doing so not only expands the analysis capabilities of RNNs, but also imparts several computational advantages.

Firstly, a key problem in the training of recurrent machine learning architectures is the difficulty that these methods have to model long term dependencies in the data in a stable way. Various approaches to improve the learning performance on long term dependencies exist, the most common being gating mechanisms as used in LSTM [13] or GRU [4]. Alternative approaches are built around norm preserving weight matrices [1, 15, 34] in order to stabilize the learning. However, adding a norm-preservation constraint can significantly increase the learning computational cost. Recently hybrid approaches combining gating with norm-preserving weight matrices have been proposed [18, 35].

While all these approaches help to stabilize learning and extend the memory capacity, they do little to address the underlying cause of poor long-term memory, which is that RNNs process and learn from only one time step per iteration. Reducing the number of RNN iterations required to process temporal sequences would be both beneficial and complementary to improving the long-term performance of RNNs. We propose to do so by integrating the short time Fourier transform (STFT) into RNNs and propose a novel Fourier RNN for analyzing and predicting sequences directly through the frequency domain.

More specifically, we propose a novel architecture to process segments of temporal or sequence data per RNN iteration. Since the frequency response is complex-valued, we leverage recent advances made in complex-valued networks [30] and specifically complex RNNs [1, 15, 34, 35] to serve as the foundation for our Fourier RNN. Working in the complex domain makes it possible to work with expressive yet stable weight matrices.

In our work, we show how gradients for both classification and regression tasks from the time domain can be back-propagated through the inverse STFT and STFT. This is especially beneficial for signals which are periodic or semi-periodic, as they often have very informative frequency domain representations. Our Fourier RNN is able to analyze and predict temporal sequences competitive with current time-based methods at a fraction of the computational cost.

The Fourier transform has been noted in the past for improving the computational efficiency of convolutional neural networks (CNNs) [2, 22, 31, 24, 33]. However, unlike in CNNs, where the gains come from the duality of convolution and multiplication in the space-frequency domain, the computational efficiency for our Fourier RNN comes from the fact that we process entire windows of data at a time rather than individual time steps. In addition, training recurrent architectures is known to be very memory-consuming. In cases where the state size is much larger than the window size, then our proposed approach will also lead to reduced memory consumption and run-time.

Our contributions can be summarize as follows:

- We propose a novel RNN architecture for analyzing (temporal) sequences using the STFT and its inverse; to the best of our knowledge, we are the first to combine STFTs and RNNs into a common framework and show how it can be applied to both classification and regression problems.
- We demonstrate how our formulation of the regression problem significantly improves efficiency and can reduce overall training time.
- We demonstrate the strengths of Fourier representations for sequence prediction on both synthetic and real-world data and achieve state of the art results for predicting human motion data.

We begin by outlining the theory of the short time Fourier transform in Section 3 and then explain how the STFT can be integrated into a complex-valued RNN in section 4.2. Finally, we demonstrate the performance of our Fourier RNN in Section 5 through a series of experiments on both synthetic and real world data.

## 2 Related Works

The analysis of time series in the frequency domain dates back to the early 1800s [10]. Fourier analysis is a staple in a broad swatch of engineering disciplines and is so ubiquitous that the Fast Fourier Transform has been described as the “*most important numerical algorithm of our lifetime*” [27].

In machine learning, Fourier analysis is mostly associated with signal-processing heavy domains such as speech recognition [3], medical imaging [32] and audio-processing [6, 29]. Recently, a comparison [11] of the time versus frequency domain for audio event recognition with neural networks showed the discriminative gains of processing sound in the frequency domain.

Within the deep learning community, the discrete Fourier transform has long been touted as a computationally efficient alternative to convolution, since convolution in time and space is equivalent to multiplication in the frequency domain. Such gains are especially relevant for convolutional neural networks in 2D [2, 22, 31, 24] and even more so in 3D [33]. In addition, Fourier-based pooling as an alternative to max-pooling [25, 26] has been explored for CNNs.

Generally, in both audio processing and speech recognition, only the magnitude of a frequency domain signal is processed, while the phase gets discarded [3, 29]. One likely reason for this is the fact that many machine learning methods and toolboxes are not designed to natively handle complex data. However, recent works in complex-valued networks [1, 7, 30, 35] makes it now possible process data fully in the frequency domain. The complex CNN presented in [30] explores complex convolutions and applies them to the Fourier spectrum of music data, whereas in [35], a complex gated RNN was applied to similar data.

## 3 Short Time Fourier Transform

### 3.1 Discrete Fourier Transform

The Fourier transform maps a signal into the spectral or frequency domain by decomposing it into a linear combination of periodic waveforms, specifically sinusoids. Analyzing signals in the spectral domain with the Fourier transform is a fundamental tool in engineering [23]. For the uninitiated reader, the discrete Fourier transform  $\mathcal{F}$  for a (discrete) signal  $\mathbf{x}$  is defined as

$$\mathbf{X}(\omega) = \mathcal{F}(\mathbf{x}) = \sum_{l=-\infty}^{\infty} \mathbf{x}[l]e^{-j\omega l}, \quad (1)$$

where  $l$  is the (time) signal index<sup>1</sup>,  $\omega$  denotes the frequency,  $e$  the exponential function and  $j = \sqrt{-1}$ . As such, the Fourier transform  $\mathbf{X}[\omega]$  is complex-valued, *i.e.*  $X[\omega] \in \mathbb{C}$ .

One can recover the signal  $\mathbf{x}$  from  $\mathbf{X}$  by taking the inverse discrete Fourier transform  $\mathcal{F}^{-1}$ , *i.e.*

$$x(l) = \mathcal{F}^{-1}(\mathbf{x}) = \sum_{l=-\infty}^{\infty} \mathbf{X}[l]e^{j\omega l}, \quad (2)$$

### 3.2 STFT

Note that in the definition given by Eq. 1, one needs infinite support of the input signal in time to estimate the frequency response according to the Fourier transform. For many real-world applications, however, including those which we wish to model with RNNs, this requirement is not only infeasible, but also it is necessary to obtain insights into changes in the frequency spectrum as function of time or signal index. To do so, one can partition the signal into overlapping segments and approximating the Fourier transform of each segment separately. This is the core idea behind the short time Fourier transform (STFT), which is used to determine a signal's frequency domain representations as it changes over time.

More formally, given a signal  $\mathbf{x}$ , we can partition it into  $n_s$  segments of length  $T$ , extracted every  $S$  time steps. The STFT  $\mathcal{F}_s$  of  $\mathbf{x}$  is defined by [5] as the discrete Fourier transform of segments of  $\mathbf{x}$ , *i.e.*

$$\begin{aligned} \mathbf{X}_m(\omega, Sm) &= \mathcal{F}_s(\mathbf{x}) = \mathcal{F}(\mathbf{w}[Sm - l]\mathbf{x}[l]) \\ &= \sum_{l=-\infty}^{\infty} \mathbf{w}[Sm - l]\mathbf{x}[l]e^{-j\omega l}, \end{aligned} \quad (3)$$

where segments of  $\mathbf{x}$  are multiplied with the windowing function  $\mathbf{w}$  with windowing index  $m$ . The simplest windowing function is rectangular, and simply extracts the signal  $\mathbf{x}$  in its original form. However, the sharp drop-off at the edge of a rectangular window requires infinite spectral support and as such, a smooth window which tapers off at the edge, such as the Hann window (see Fig. 1) is recommended instead [8]:

$$w_{\text{Hann}}[n] = \sin^2\left(\frac{\pi n}{N-1}\right), \quad (4)$$

where  $N$  is the length of the window function and is equal to  $T$ , the segment length which we wish to extract.

Denoting some segment of  $\mathbf{x}$  as  $\mathbf{x}_s$ , Equation 3 is generally implemented in practice by taking the fast Fourier Transform (FFT)<sup>2</sup> of  $\mathbf{x}_s$  multiplied by the window  $\mathbf{w}$ . Again, due to the multiplication with  $e^{j\omega l}$ , the resulting transform  $\mathbf{X}_m$  is a complex valued.

Supposing now that we are given some frequency signal  $\hat{\mathbf{X}}_m$ . The time signal  $\hat{\mathbf{x}}$  represented by  $\hat{\mathbf{X}}$  can be recovered with the inverse short time Fourier transform (iSTFT)  $\mathcal{F}_s^{-1}$  and is defined by [5] as:

$$\begin{aligned} \hat{\mathbf{x}}_w &= \mathcal{F}_s^{-1}(\mathbf{X}_m(n), Sm) \\ &= \frac{\sum_{m=-\infty}^{\infty} \mathbf{w}(Sm - n)\hat{\mathbf{x}}_w(Sm, n)}{\sum_{m=-\infty}^{\infty} \mathbf{w}^2(Sm, n)}, \end{aligned} \quad (5)$$

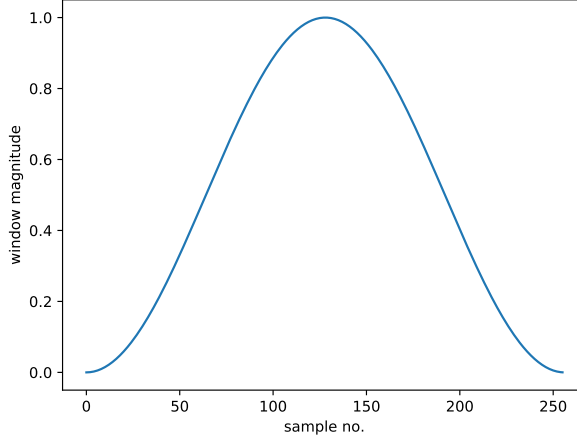
where the signal  $\hat{\mathbf{x}}_w$  is the inverse Fourier transform of  $\mathbf{X}_w$

$$\hat{\mathbf{x}}_w = \frac{1}{T} \sum_{l=-\infty}^{\infty} \mathbf{X}_m(Sm, l)e^{j\omega l} \quad (6)$$

with  $l$  running along the frequency dimension of  $X_m$ . Equation 5 undoes the effect of the windowing function. Implementations of the iSTFT in Equation 5 require careful treatment of the denominator; to avoid division by values close to zero, a common strategy is to add a small tolerance  $\epsilon = 0.001$ . When evaluating equation 5,  $Sm$  generally evaluates to an integer smaller than the window size  $T$  and subsequent elements in the sum overlap, hence the alternative naming of it being an “*overlap and add*” method.

<sup>1</sup>Out of convenience, we will refer to the signal index interchangeably as time, though  $l$  can denote any other evenly spaced signal index as well.

<sup>2</sup>The FFT refers to any fast algorithmic implementation of the discrete Fourier transform

Figure 1: A plot of the Hann-window function  $w$ .

## 4 Fourier Recurrent Neural Networks

### 4.1 Basic RNN

We begin by defining a real-valued basic recurrent neural network (RNN) as follows:

$$\mathbf{z}_t = \mathbf{W}\mathbf{h}_{t-1} + \mathbf{V}\mathbf{x}_t + \mathbf{b} \quad (7)$$

$$\mathbf{h}_t = f_a(\mathbf{z}_t) \quad (8)$$

$$\mathbf{y}_t = \mathbf{W}_p\mathbf{h}_t \quad (9)$$

The input, hidden unit and output vectors are given respectively by  $\mathbf{x}_t \in \mathbb{R}^{1 \times 1}$ ,  $\mathbf{h}_t \in \mathbb{R}^{n_h \times 1}$  and  $\mathbf{y}_t \in \mathbb{R}^{n_y \times 1}$  at time  $t$  where  $n_x$ ,  $n_h$  and  $n_y$  are the dimensionalities of the input, hidden and output states respectively. The function  $f_a$  is a non-linear activation; hyperbolic tangents are a common choice for RNNs. The network weights are defined as real-valued matrices, *i.e.*  $\mathbf{W} \in \mathbb{R}^{n_h \times n_h}$ ,  $\mathbf{V} \in \mathbb{R}^{n_h \times n_x}$ ,  $\mathbf{b} \in \mathbb{R}^{n_h \times 1}$  and  $\mathbf{W}_p \in \mathbb{R}^{n_h \times n_y}$ .

For regression to a target vector  $\mathbf{y}_t^{\text{gt}}$ , one can define the mean squared error (MSE) loss as

$$l_{mse} = 1/n_y \sum_{l=0}^{n_y} (\mathbf{y}_t[l] - \mathbf{y}_t^{\text{gt}}[l])^2. \quad (10)$$

For classification, one can convert  $\mathbf{y}_t$  into a label  $\mathbf{y}_c$  based on the standard softmax and apply the standard cross-entropy loss with ground truth labels  $c$ :

$$l_{ce} = - \sum_{l=1}^{n_y} \mathbf{c} \log(\mathbf{y}_c[l]) + (1 - \mathbf{c}) \log(1 - \mathbf{y}_c[l]). \quad (11)$$

### 4.2 Fourier RNN

We can move RNN processing into the frequency domain and define our Fourier RNN (fRNN) by applying the STFT to the input signal  $x$ . Assuming that a projection of the final hidden vector is also signal of the temporal domain, we can apply the iSTFT to recover the output  $y$ . This can be summarized by the following set of RNN equations:

$$\mathbf{X}_\tau = \mathcal{F}(\{\mathbf{x}_{S\tau-T/2}, \dots, \mathbf{x}_{S\tau+T/2}\}) \quad (12)$$

$$\mathbf{z}_\tau = \mathbf{W}_c\mathbf{h}_{\tau-1} + \mathbf{V}_c\mathbf{X}_\tau + \mathbf{b}_c \quad (13)$$

$$\mathbf{h}_\tau = f_a(\mathbf{z}_\tau) \quad (14)$$

$$\mathbf{y}_\tau = \mathcal{F}^{-1}(\{\mathbf{W}_{pc}\mathbf{h}_0, \dots, \mathbf{W}_{pc}\mathbf{h}_\tau\}) \quad (15)$$

where  $\tau = [0, n_s]$ , *i.e.* from zero to the total number of segments  $n_s$ . The output  $y_\tau$  may be computed based on the available outputs  $\{\mathbf{W}_p\mathbf{h}_0, \dots, \mathbf{W}_p\mathbf{h}_\tau\}$  at step  $\tau$  once all  $n_s$  processing steps are done and all  $\mathbf{h}$  are available.

Note that even though equations 13 to 15 are exactly analogous to the basic RNN in equations 7 to 9, the change from  $\mathbf{x}_t$  to  $\mathbf{X}_\tau$  has two key implications. First of all, because  $\mathbf{X}_\tau \in \mathbb{C}^{n_f \times 1}$  is a complex signal, the hidden state as well as subsequent weight matrices all become complex, *i.e.*  $\mathbf{h}_\tau \in \mathbb{C}^{n_h \times 1}$ ,  $\mathbf{W}_c \in \mathbb{C}^{n_h \times n_h}$ ,  $\mathbf{V}_c \in \mathbb{C}^{n_h \times n_f}$ ,  $\mathbf{b}_c \in \mathbb{C}^{n_h \times 1}$  and  $\mathbf{W}_{pc} \in \mathbb{C}^{n_h \times n_f}$ , where  $n_h$  is the hidden size of the networks as before and  $n_f$  is the number of frequencies in the STFT.

Having complex-valued states necessitates the use of a complex non-linear activation function. Two possible choices are analogues of the tanh and ReLU in the complex domain. The first, popularized by Hirose [12] is defined as

$$f_{\text{Hirose}}(z) = \tanh\left(\frac{|z|}{m}\right) \frac{z}{|z|}, \quad (16)$$

where  $z$  indicates a complex input,  $|z|$  is its magnitude and  $m$  is a scaling factor. A more recently proposed alternative is the modReLU [1], defined as

$$f_{\text{modReLU}}(z) = \text{ReLU}(|z| + b) \frac{z}{|z|}, \quad (17)$$

where  $b$  is a scalar offset.

The second implication to note is that the step index in the fRNN, by changing from  $t$  to  $\tau$ , means that the fRNN effectively covers  $S$  time steps of the standard RNN per step. This has significant bearing on the overall memory consumption as well as the computational cost, both of which influence the overall network training time. Considering only the multiplication of the state matrix  $\mathbf{W}_c$  and the state vector  $\mathbf{h}_\tau$ , which is the most expensive operation, the basic RNN requires  $N \cdot O(n_h^3)$  operations for  $N$  total time steps. When using the Fourier RNN with an FFT implementation of the STFT, one requires only  $N/S \cdot (O(T \log T) + O(n_h^3))$ , where the  $T \log T$  term comes from the FFT operation. The architectural changes lead to larger input layers and fewer RNN iterations.  $\mathbf{X}$  is higher dimensional than  $\mathbf{x}$ , but we save on overall computation is the step size is large enough which will make  $N/S$  much smaller than  $N$ .

We can generalise the approach described above into:

$$\mathbf{X}_\tau = \mathcal{F}(\{\mathbf{x}_{S\tau-T/2}, \dots, \mathbf{x}_{S\tau+T/2}\}) \quad (18)$$

$$\mathbf{h}_t = \text{RNN}_{\mathbb{C}}(\mathbf{X}_\tau, \mathbf{h}_{t-1}) \quad (19)$$

$$\mathbf{y}_t = \mathcal{F}^{-1}(\{\mathbf{W}_{pc}\mathbf{h}_0, \dots, \mathbf{W}_{pc}\mathbf{h}_\tau\}), \quad (20)$$

where instead of the basic formulation outlined above, more sophisticated complex RNN-architectures [1, 34, 35] represented by  $\text{RNN}_{\mathbb{C}}$  may be substituted.

### 4.3 Loss Functions

For classification tasks, one can bypass the inverse STFT step defined in Equation 18 and directly map the complex fRNN-state to real values, *e.g.* via a simple splitting of the real and imaginary components [1]:

$$\mathbf{y}_t = \mathbf{U} \begin{pmatrix} \Re(\mathbf{h}_t) \\ \Im(\mathbf{h}_t) \end{pmatrix} + \mathbf{b}_o, \quad (21)$$

with the real projection matrix  $\mathbf{U} \in \mathbb{R}^n$ . The output  $\mathbf{y}_t$  can then be converted into a class label and the standard cross-entropy loss as given in equation 11 can be applied.

For regression problems, time and frequency loss-representations may be considered. A time-based loss such as an MSE as described in equation 10 over time requires backpropagation through the iSTFT. A second approach is to project the ground truth sequence into the frequency domain  $\mathbf{Y}_\tau = \mathcal{F}(\{\mathbf{y}_{S\tau-T/2}, \dots, \mathbf{y}_{S\tau+T/2}\})$  and define a mean squared error analogously to the time domain definition on the real and imaginary parts,

$$\begin{aligned} c_{f\text{-mse}}(\mathbf{Y}_\tau, \mathbf{Y}_\tau^{gt}) &= \sum_{l=0}^{n_y} \Re(\mathbf{Y}_\tau[l] - \mathbf{Y}_\tau^{gt}[l])^2 \\ &+ \sum_{l=0}^{n_y} \Im(\mathbf{Y}_\tau[l] - \mathbf{Y}_\tau^{gt}[l])^2, \end{aligned} \quad (22)$$

During our experimentation, we observed small oscillations of the resulting predictions, which we believe are caused by small errors in the high frequency components of the frequency domain predictions, which often have ground truth values very close to zero.

To minimize these effects, we advocate applying a log-scaling to the frequency components, so as to increase the contributions of the higher-frequency components in the loss:

$$c_{\text{ln-mse}}(\mathbf{Y}_\tau, \mathbf{Y}_\tau^{gt}) = \sum_{l=0}^{n_y} \log(\Re(\mathbf{Y}_t[l] - \mathbf{Y}_t^{gt}[l])^2), \quad (23)$$

$$+ \sum_{l=0}^{n_y} \log(\Im(\mathbf{Y}_t[l] - \mathbf{Y}_t^{gt}[l])^2).$$

In our experiments we explore possible combinations of these formulations:

$$l_{\text{tot}} = \lambda_c(c_{f\text{-mse}} + \lambda_f c_{\text{ln-mse}}) + c_{t\text{-mse}} \quad (24)$$

The weighting constants lambda are used to scale the terms and weigh their impact on the training procedure.

#### 4.4 Complex-Convolutions

Given a complex input vector  $\mathbf{h} = \mathbf{x} + i\mathbf{y}$  and a complex kernel  $\mathbf{W} = \mathbf{A} + i\mathbf{B}$ , following [30] complex convolutions may be implemented using:

$$\mathbf{W} * \mathbf{h} = (\mathbf{A} * \mathbf{x} - \mathbf{B} * \mathbf{y}) + i(\mathbf{B} * \mathbf{x} + \mathbf{A} * \mathbf{y}) \quad (25)$$

Which may be represented in terms of matrix multiplications as [30]:

$$\begin{pmatrix} \Re(\mathbf{W} * \mathbf{h}) \\ \Im(\mathbf{W} * \mathbf{h}) \end{pmatrix} = \begin{pmatrix} \mathbf{A} & -\mathbf{B} \\ \mathbf{B} & \mathbf{A} \end{pmatrix} * \begin{pmatrix} \mathbf{x} \\ \mathbf{y} \end{pmatrix} \quad (26)$$

We use the complex convolutions as an input pre-processing layer in the frequency domain in order to extract frequency domain features, which we feed into a complex RNN for processing.

## 5 Experimentation

### 5.1 Lorenz Attractor

We start by demonstrating the Fourier RNN on a synthetic Lorenz-system, which generates data similar to real-world laser data observed in [14]. A 3D Lorenz attractor can be defined as

$$\begin{aligned} \frac{dx}{dt} &= \sigma(y - x), \\ \frac{dy}{dt} &= x(\rho - z) - y, \\ \frac{dz}{dt} &= xy - \beta z, \end{aligned} \quad (27)$$

where we use constant parameters  $\sigma = 10$ ,  $\rho = 28$  and  $\beta = 8/3$ . We simulate the Lorenz equations using a simple forward-Euler simulation scheme, using randomly perturbed initial conditions:

$$\mathbf{s}_{t+1} = \mathbf{s}_t + \gamma \cdot \left[ \frac{dx}{dt} \quad \frac{dy}{dt} \quad \frac{dz}{dt} \right]^T, \quad (28)$$

with  $\mathbf{s} = [x \ y \ z]^T$  and  $\gamma = 0.01$  is the step size.

This system is chaotic in nature. When the precise initial conditions are unknown, it is impossible for a machine learning algorithm to perfectly simulate the system being trained on data only. The chaotic property, combined with the fact that the system is pseudo-periodic, makes it an interesting test-bed for our Fourier RNN, because we can compare the predictions of different approaches vs. the simulated ground-truth over time. For simplicity, we predict  $x^2$ ; one example sequence is shown in figure 3 (a).

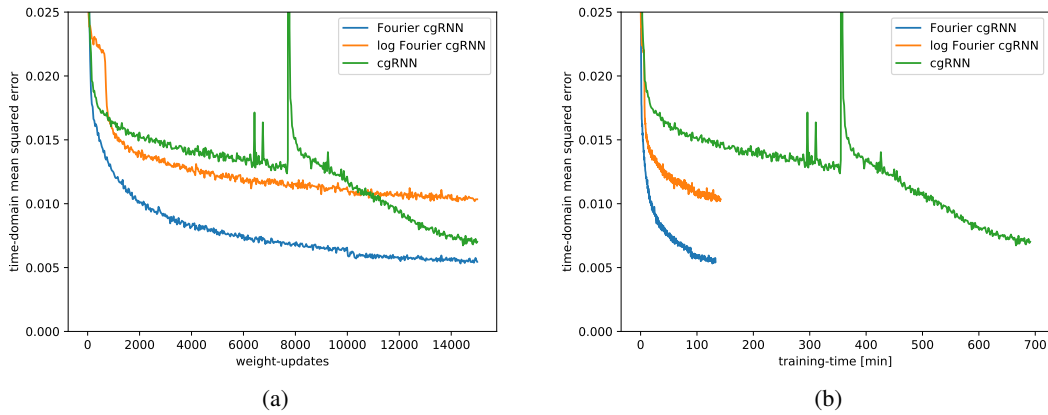


Figure 2: Time domain loss vs. weights updates (a). Time domain loss vs. overall training runtime (b).

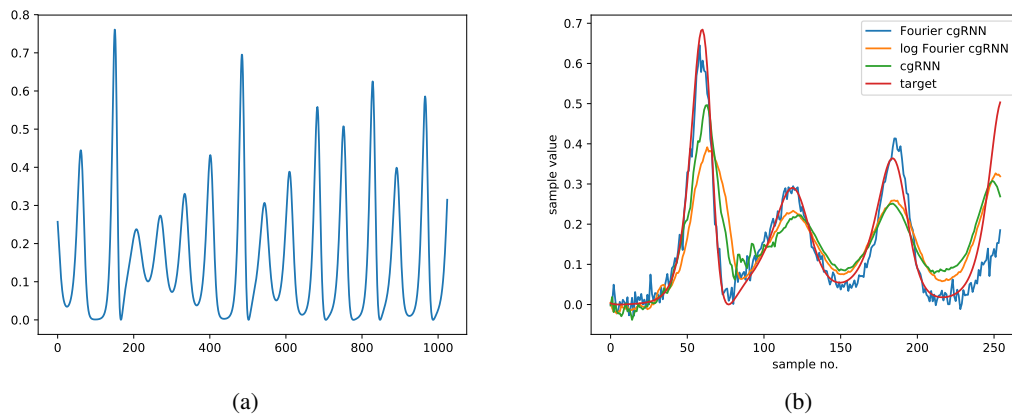


Figure 3:  $x^2$  computed through the Lorenz equations (a). Prediction performance of the models shown in time and freq domain (b).

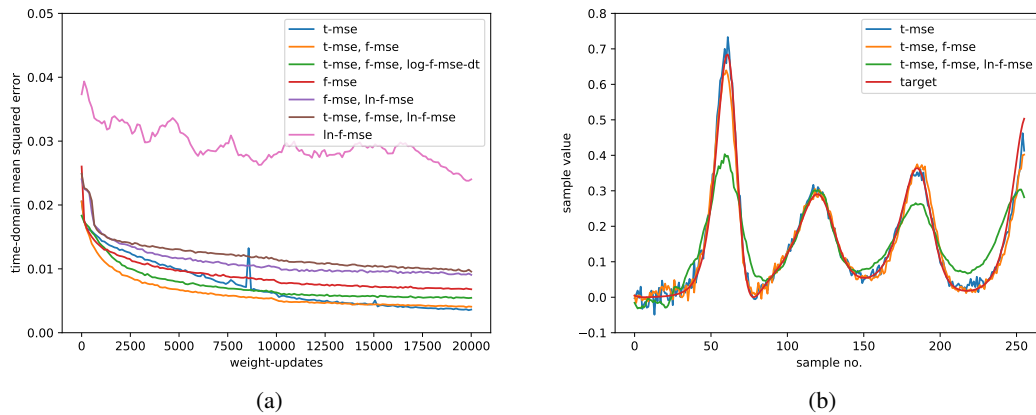


Figure 4: Convergence of various loss formulations (a) and resulting fit of selected models (b).

### 5.1.1 Lorenz-Results

We work with the generalized Fourier RNN as described in section 4.2, with the complex GRU cell introduced in [35] as the base RNN and compare to a time-domain variant of the same base RNN. For fairness in comparison, we keep the both networks balanced at around 410k parameters with a batch size of 250 and set the learning rate to 0.001. Of 1024 Lorenz samples, we encode 768 samples and predict the following 256, using the same cell for both encoding and prediction.

**Convergence** For the Fourier networks, the window size is set to 32 and the cell size is set to 250. All networks are trained for 15k iterations. The Fourier-domain networks use a combined time and frequency domain loss as described in Equation 24 using  $\lambda_f = 0, \lambda_f = 1e4$  (AY: ?) and  $\lambda_c = 1e - 2, \lambda_c = 1e - 3$  for the purely linearly scaled experiment and the log scaled additional term respectively. To offset the extra parameters the Fourier networks use to process the larger inputs, the time domain network is given a state size of 260, which leads to approximately equal weights. The time domain MSE vs. the number of training iterations for different variations of the loss function are shown in Figure 2 (a). The network using frequency and temporal domain mean squared error converges the fastest. A closer look at figure 2 reveals that log scaling of the frequency domain loss removes the high-frequency artifacts, but leads to slower convergence and as a result is less accurate. The number of iterations or weight-updates does not fully represent the benefits of working in the Fourier domain; in comparison to the time-based cgRNN, each iteration of the Fourier update is significantly faster and as a result, the overall training time is roughly one seventh (see Figure 2 (b)).

**Loss Formulations** In Figure 4 we explore the effect of various loss formulations. We repeat the previous experiment, while increasing the total number of iterations to 20000. We run the following experiments:

- Using time domain mse only (t-mse,  $\lambda_f = 0, \lambda_c = 0$ )
- A frequency time mse (t-mse, fmse,  $\lambda_f = 0, \lambda_c = 1e - 2$ )
- Additional log-scaling in the frequency domain (t-mse, fmse, log-f-mse,  $\lambda_f = 1e4, \lambda_c = 1e - 3$ )
- Step dependent log scaling scaling (t-mse, fmse, log-f-mse-dt,  $\lambda_f = 1e4 \frac{s}{s_{tot}}, \lambda_c = 1e - 3$  where  $s$  denotes the current step number and  $s_{tot}$  the total number of iterations).
- Time domain mse and log-scaling (t-mse, fmse, log-f-mse-dt,  $\lambda_f = 1e4 \frac{s}{s_{tot}}, \lambda_c = 1e - 3$ , without  $c_{f-mse}$ )
- log-scale loss  $c_{ln-mse}$  only (ln-mse).

We conclude that a linearly scaled frequency domain loss is most beneficial for convergence properties, *i.e.* quick and accurate. However, as shown in Figures 2(b) and 4 (b), such a term stand-alone leads to high-frequency artifacts.

Adding a log scaling in the frequency domain solves this problem but can slow down convergence so the two must be balanced to control the trade-off between minimizing noise and maintaining a quick convergence.

Having observed faster initial convergence, we believe these results are an indication, that frequency domain representations are beneficial in scenarios where few training data is available.

## 5.2 Human Motion Prediction

We test our architecture on the task of predicting three dimensional human motion sequences. Given a series of poses the task is to predict future poses. We work with Mocap pose-data from the Human 3.6M data-set [16]. The pre-processing converts the motion capture into exponential map representations of each joint. We hold back the data from actor five for testing and train on the data from the remaining six of the seven actors [17][21]. We first encode 36 samples which span 1.5 seconds of motion. Based on the encoding 24 samples or one second of motion are predicted. We use euclidean distance in Euler angles with respect to the ground truth poses as evaluation metric.

Table 1: Comparison of our cgRNN with the convSeq2Seq [20] on human motion prediction.

Action	fft-cgRNN					convSeq2Seq [20]				
	80ms	160 ms	320ms	400ms	1000ms	80ms	160ms	320ms	400ms	1000ms
walking	<b>0.22</b>	<b>0.43</b>	<b>0.64</b>	<b>0.66</b>	1.10	0.33	0.54	0.68	0.73	<b>0.92</b>
eating	<b>0.22</b>	0.41	0.6	0.72	1.27	<b>0.22</b>	<b>0.36</b>	<b>0.58</b>	<b>0.71</b>	<b>1.24</b>
smoking	<b>0.25</b>	0.61	<b>0.83</b>	<b>0.88</b>	1.75	0.26	<b>0.49</b>	0.96	0.92	<b>1.62</b>
discussion	<b>0.24</b>	<b>0.66</b>	<b>0.84</b>	<b>0.87</b>	<b>1.71</b>	0.32	0.67	0.94	1.01	1.86
directions	<b>0.28</b>	<b>0.56</b>	<b>0.76</b>	<b>0.83</b>	1.48	0.39	0.60	0.80	0.91	<b>1.45</b>
greeting	<b>0.33</b>	<b>0.62</b>	<b>1.11</b>	<b>1.18</b>	1.86	0.51	0.82	1.21	1.38	<b>1.72</b>
phoning	<b>0.57</b>	<b>0.80</b>	<b>1.46</b>	<b>1.59</b>	<b>1.72</b>	<b>0.59</b>	1.13	1.51	1.65	1.81
posing	0.59	0.83	1.34	1.48	<b>2.3</b>	<b>0.29</b>	<b>0.60</b>	<b>1.12</b>	<b>1.37</b>	2.65
purchases	<b>0.37</b>	<b>0.6</b>	<b>1.04</b>	<b>1.07</b>	<b>2.22</b>	0.63	0.91	1.19	1.29	2.52
sitting	<b>0.31</b>	0.7	<b>0.94</b>	<b>1.11</b>	1.89	0.39	<b>0.61</b>	1.02	1.18	<b>1.67</b>
sitting down	<b>0.39</b>	0.88	<b>1.15</b>	<b>1.23</b>	2.28	0.41	<b>0.78</b>	1.16	1.31	<b>2.06</b>
taking photo	<b>0.23</b>	0.60	<b>0.72</b>	<b>0.81</b>	<b>1.3</b>	<b>0.23</b>	<b>0.49</b>	0.88	1.06	1.4
waiting	<b>0.25</b>	<b>0.54</b>	<b>1.03</b>	<b>1.14</b>	<b>2.29</b>	0.3	0.62	1.09	1.30	2.5
walking dog	<b>0.35</b>	<b>0.66</b>	<b>1.15</b>	<b>1.25</b>	1.95	0.59	1.00	1.32	1.44	<b>1.92</b>
walking together	<b>0.21</b>	<b>0.48</b>	0.72	<b>0.70</b>	1.40	0.27	0.52	<b>0.71</b>	0.74	<b>1.28</b>

Our fft-cgRNN ( $n_h = 512$ ,  $w_s = 12$ ) predicts human motions which are either comparable or slightly better than convolution-based approach [20].

In this section we explore human motion prediction in the frequency domain. We choose our window size to be 12 samples covering half a second of movement, we move the window along the sequence in steps of six samples which leads to a window overlap of 6 samples. We process 16 batches at a time and work with a learning rate of 0.005 and a cell-size of 512 and a time domain based loss. We introduce residual connections into our framework similar to [21]. This amounts to modelling only the change of the spectrum instead of having to reconstruct it from scratch at every time step. By using residual connections we assume that the movement under consideration will repeat in the next window in a similar fashion, for periodic movements this should require only small changes to the spectrum. We model these changes using the complex GRU as described in [35].

Table 5.2 shows our results in comparison to the results published in [20]. We observe that our frequency domain approach does very well in the short term with mixed results for longer term predictions.

### 5.3 Music Analysis

Music transcription is concerned with determining what each instrument is playing in a recording. The music net data-set [29] consists of 330 classical music recordings. The transcription problem is expressed as a multi-label classification problem. By generating a label vector  $y \in \{0, 1\}^{128}$  the network determines the active keys in the corresponding midi file. The wave-form files are split into 327 training and 3 testing data sets. The recordings which are sampled at 11kHz are segmented into windows of 2048 samples each. We move the segments forward using a step size of 512 samples. The STFT of each window is computed, the resulting output is processed by a complex neural network.

Table 2: Previously published end-to-end music transcription results as well as our result for comparison.

Model	Avg.Prec.
deep complex [30]	72.9
channel convolution [28]	73.3
complex convolutional-RNN [ours]	73.8

After the STFT output we combine complex convolutions as described by [30] with complex recurrent structures [35]. We use the convolutions to extract features, which we integrate in time using the RNN. We use four convolutional layers of width 12,9,9,6 with strides 4,3,3,2 and depths 32,64,128,128 followed by a bidirectional complex GRU layer of size 1024 and a final complex GRU of the same size, which integrates the bidirectional features into the final output. We train for 400k iterations using a learning rate of 0.0001 and use a step-wise exponential learning rate decay, which decays the learning rate every 50000 steps using a decay rate of 0.9. The complex STFT convolutional GRU combination outperforms previous end-to-end approaches, because it is the first to use information from previous and future frames as well as convolutional features. It does not beat the partially hand crafted wide-layer network proposed recently in [28], which was trained using data augmentation techniques we did not employ.

## 6 Conclusion

In this paper we presented a frequency domain recurrent sequential data analysis and prediction framework, which we believe makes a significant addition to the complex domain machine learning framework previously presented in [30] [34] [35] and other works. We hope that our contribution will encourage additional research in the future in particular on the combination with filtering algorithms and frequency domain convolutions, which we believe have the potential to smooth the predictions we obtained in this work and unlock the full potential of future frequency domain machine learning methods.

## References

- [1] M. Arjovsky, A. Shah, and Y. Bengio. Unitary evolution recurrent neural networks. In *ICML*, 2016.
- [2] Y. Bengio, Y. LeCun, et al. Scaling learning algorithms towards ai. *Large-scale kernel machines*, 34(5):1–41, 2007.
- [3] W. Chan, N. Jaitly, Q. Le, and O. Vinyals. Listen, attend and spell: A neural network for large vocabulary conversational speech recognition. In *Acoustics, Speech and Signal Processing (ICASSP), 2016 IEEE International Conference on*, pages 4960–4964. IEEE, 2016.
- [4] K. Cho, B. van Merriënboer, aglar Gülehre, D. Bahdanau, F. Bougares, H. Schwenk, and Y. Bengio. Learning phrase representations using rnn encoder-decoder for statistical machine translation. In *EMNLP*, 2014.
- [5] J. L. D. Griffin. Signal estimation from modified short-time fourier transform. In *IEEE Transactions on Acoustics, Speech, and Signal Processing*, 1984.
- [6] S. Dieleman and B. Schrauwen. End-to-end learning for music audio. In *Acoustics, Speech and Signal Processing (ICASSP), 2014 IEEE International Conference on*, pages 6964–6968. IEEE, 2014.
- [7] N. Guberman. On complex valued convolutional neural networks. Technical report, The Hebrew University of Jerusalem Israel, 2016.
- [8] F. Harris. On the use of windows for harmonic analysis with the discrete fourier transform. In *Proceedings of the IEEE*, 1978.
- [9] W. Hayt, J. E. Kemmerly, and S. M. Durbin. *Engineering Circuit Analysis*. McGraw-Hill Education - Europe, 2011.
- [10] M. Heideman, D. Johnson, and C. Burrus. Gauss and the history of the fast fourier transform. *IEEE ASSP Magazine*, 1(4):14–21, 1984.
- [11] L. Hertel, H. Phan, and A. Mertins. Comparing time and frequency domain for audio event recognition using deep learning. In *Neural Networks (IJCNN), 2016 International Joint Conference on*, pages 3407–3411. IEEE, 2016.
- [12] A. Hirose. *Complex-valued neural networks: Advances and applications*. John Wiley & Sons, 2013.
- [13] S. Hochreiter and J. Schmidhuber. Long short term memory. *Neural Computation*, 1997.
- [14] U. Huebner, N. Abraham, and C. Weiss. Dimensions and entropies of chaotic intensity pulsations in a single-mode far-infrared nh3 laser. In *PhysRevA*, 1989.
- [15] S. Hyland and G. Rätsch. Learning unitary operators with help from  $u(n)$ . In *AAAI*, 2017.
- [16] C. Ionescu, D. Papava, V. Olaru, and C. Sminchisescu. Human3.6M: Large Scale Datasets and Predictive Methods for 3D Human Sensing in Natural Environments. *IEEE Trans. Pattern Analysis and Machine Intelligence*, 36(7):1325–1339, jul 2014.
- [17] A. Jain, A. Zamir, S. Savarese, and A. Saxena. Structural-RNN: Deep learning on spatio-temporal graphs. In *CVPR*, 2016.
- [18] L. Jing, C. Gulcehre, J. Peurifoy, Y. Shen, M. Tegmark, M. Solja, and Y. Bengio. Gated orthogonal recurrent units: On learning to forget. In *AAAI Workshops*, 2018.
- [19] V. Komornik and P. Loret. *Fourier Series in Control Theory*. Springer Monographs in Mathematics, 2005.
- [20] C. Li, Z. Zhang, W. S. Lee, and G. H. Lee. Convolutional sequence to sequence model for human dynamics. In *Proceedings of the IEEE Conference on Computer Vision and Pattern Recognition*, pages 5226–5234, 2018.
- [21] J. Martinez, M. Black, and J. Romero. On human motion prediction using recurrent neural networks. In *CVPR*, 2017.
- [22] M. Mathieu, M. Henaff, and Y. LeCun. Fast training of convolutional networks through ffts. *arXiv preprint arXiv:1312.5851*, 2013.
- [23] R. Pintelon and J. Schoukens. *System identification: A frequency domain approach*. John Wiley & Sons, 2012.
- [24] H. Pratt, B. Williams, F. Coenen, and Y. Zheng. FCNN: fourier convolutional neural networks. In *Joint European Conference on Machine Learning and Knowledge Discovery in Databases*, pages 786–798. Springer, 2017.
- [25] O. Rippel, J. Snoek, and R. P. Adams. Spectral representations for convolutional neural networks. In *Advances in neural information processing systems*, pages 2449–2457, 2015.
- [26] J. Ryu, M.-H. Yang, and J. Lim. Dft-based transformation invariant pooling layer for visual classification. In *ECCV*, 2018.

- [27] G. Strang. Wavelets. *American Scientist*, 82(3):250–255, 1994.
- [28] J. Thickstun, Z. Harchaoui, D. P. Foster, and S. M. Kakade. Invariances and data augmentation for supervised music transcription. In *International Conference on Acoustics, Speech, and Signal Processing (ICASSP)*, 2018.
- [29] J. Thickstun, Z. Harchaoui, and S. Kakade. Learning features of music from scratch. In *ICLR*, 2017.
- [30] C. Trabelsi, O. Bilaniuk, Y. Zhang, D. Serdyuk, S. Subramanian, J. F. Santos, S. Mehri, N. Rostamzadeh, Y. Bengio, and C. Pal. Deep complex networks. In *ICLR*, 2018.
- [31] N. Vasilache, J. Johnson, M. Mathieu, S. Chintala, S. Piantino, and Y. LeCun. Fast convolutional nets with fbfft: A gpu performance evaluation. *arXiv preprint arXiv:1412.7580*, 2014.
- [32] P. Virtue, S. Yu, and M. Lustig. Better than real: Complex-valued neural nets for MRI fingerprinting. In *ICIP*, 2017.
- [33] Z. Wang, Q. Lan, H. He, and C. Zhang. Winograd algorithm for 3d convolution neural networks. In *ICANN*, 2017.
- [34] S. Wisdom, T. Powers, J. Hershey, J. Le Roux, , and L. Atlas. Full-capacity unitary recurrent neural networks. In *NIPS*, 2016.
- [35] M. Wolter and A. Yao. Complex gated recurrent neural networks. In *Conference on Neural Information Processing Systems*, 2018.